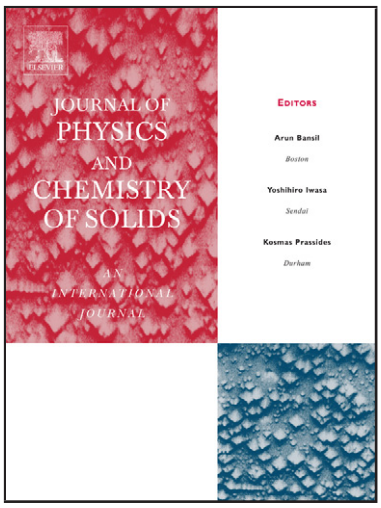

www.elsevier.com/locate/jpcs

Crystal structure, electronic and transport properties of $AgSbSe_2$ and $AgSbTe_2$

K. Wojciechowski, J. Tobola, M. Schmidt, R. Zybala

PII: S0022-3697(08)00351-X
DOI: doi:10.1016/j.jpcs.2008.06.148
Reference: PCS 5654

To appear in: *Journal of Physics and Chemistry of Solids*

Received date: 14 January 2008
Revised date: 22 May 2008
Accepted date: 30 June 2008

Cite this article as: K. Wojciechowski, J. Tobola, M. Schmidt and R. Zybala, Crystal structure, electronic and transport properties of $AgSbSe_2$ and $AgSbTe_2$, *Journal of Physics and Chemistry of Solids* (2008), doi:10.1016/j.jpcs.2008.06.148

Crystal structure, electronic and transport properties of $AgSbSe_2$ and $AgSbTe_2$

K. Wojciechowski[1*], J. Tobola[2], M. Schmidt[1], R. Zybala[1]

[1] Faculty of Materials Science and Ceramics

[2]Faculty of Physics and Applied Computer Science

AGH University of Science and Technology, Al. Mickiewicza 30, 30-059 Cracow, Poland

e-mail : gcwojcie@cyf-kr.edu.pl, phone: (+48)12-617-34-42

Abstract

Undoped and *p* and *n* doped Ag*Sb*X_2 (*X* = Se and Te) materials were synthesized by direct fusion technique. The structural properties were investigated by X-ray diffraction and SEM microscopy. The electrical conductivity, thermal conductivity and Seebeck coefficient have been measured as a function of temperature in the range from 300 to 600 K.

To enlighten electron transport behaviours observed in $AgSbSe_2$ and $AgSbTe_2$ compounds, electronic structure calculations have been performed by the Korringa-Kohn-Rostoker method as well as KKR with with coherent potential approximation (KKR-CPA) for ordered (hypothetical Ag*X* and Sb*X* as well as Ag*Sb*X_2 approximates) and disordered systems ($Ag_{1-x}Sb_xX$), respectively. The calculated density of states in the considered structural cases shows apparent tendencies to opening the energy gap near the Fermi level for the stoichiometric Ag*Sb*X_2 compositions, but a small overlap between valence and conduction bands is still present. Such electronic structure behaviour well agrees with the semi-metallic properties of the analyzed samples.

Keywords: thermoelectric materials, electronic materials, semiconductors, electronic structure, electrical properties.

* corresponding author

1. Introduction

The ternary chalcogenides $AgSbSe_2$ and $AgSbTe_2$ belongs to family of semiconductors with disordered NaCl cubic structure (s.g. Fm3m) in which silver and antimony occupy metal sublattice [1-3]. Alloys of both compounds either in single-crystal form or in thin-film form have received considerable interest owing to their optical and electronic properties. They are attractive phase-change (PC) materials used as a switching medium in rewritable optical memories [4-11].

Both compounds are also very interesting due to their thermoelectric properties (see Table1), especially very low thermal conductivity $\lambda < 1$ $Wm^{-1}K^{-1}$ which is a consequence of their disordered structure. Cubic $AgSbTe_2$ is known as a good *p*-type thermoelectric material, but due to its thermodynamical instability below 360°C it slowly decomposes to secondary phases: α-Ag_2Te and Sb_2Te_3, what limits its practical application. It is expected that alloying of $AgSbTe_2$ with other cubic compounds, such us: GeTe (so called TAGS alloys [12]), PbTe and SnTe, can help to stabilize the NaCl structure. However, these alloys are also known to be complicated by their inhomogeneity, despite reports of complete solid solutions in phase diagram determinations [13]. Exceptionally high thermoelectric figure of merit $ZT = 2$, has been reported for $(Ag_{1-y}SbTe_2)_{0.05}$ $(PbTe)_{0.95}$, which may involve the nanoscale second-phase inclusions. Authors believe that these inclusions are responsible for quantum effects increasing thermoelectric figure of merit *ZT*. Although, conflicting reports on the same materials claim only *ZT* of 1 or less. Chen *et al.* [13] have shown that these materials are multiphase on the scale of millimetres despite appearing homogeneous by *X*-ray diffraction and routine electron microscopy. Using a scanning Seebeck microprobe, authors found significant variation of Seebeck coefficient including both *n*-type and *p*-type behaviour in the same sample. It can not be excluded that complicated behaviour of the alloys can be result of the complex nature of their parent compounds.

Despite that $AgSbSe_2$ and $AgSbTe_2$ based materials are widely investigated, the basic information about properties of pure compounds, e.g. the nature of the disorder or electronic structure is still not quite clear.

2. Experimental and theoretical details

The starting materials were prepared by direct fusion of stoichiometric amounts of their constituent elements (Ag, Sb, Se, Te) of purity 99.99% in sealed, evacuated silica tubes covered inside with thin layer of pyrolytical carbon. Tubes were heated in temperature controlled, cradled furnace at 700°C for 1 h, with continuous swinging to complete mixing and reaction. Tubes were gradually cooled to room temperature to obtain polycrystalline ingots. The materials were ground and hot-pressed in graphite dies (argon atmosphere, t = 20 min, p = 30 MPa, at T = 410 °C) and slowly cooled down with rate of 1 °C/min to the room temperature in order to avoid fracturing. Because $AgSbTe_2$ can undergo decomposition below 360°C some of $AgSbTe_2$ samples were heated in evacuated quartz ampoules to 450°C and rapidly cooled down by quenching in water, in order to obtain single-phased materials. The samples of 10 mm in diameter and about 20 mm in height, were cut with a diamond saw and polished.

The prepared materials were characterized by X-ray diffractometer (X'Peret Philips system, with filtered CuK_α radiation) and scanning electron microscopy (JEOL JSM-840) with an electron-probe microanalysis apparatus (EPMA). The lattice parameters were calculated from the experimental X-ray patterns using *FullProf* refinement program implementing Rietveld method. Mass densities were determined using the immersion technique with water as the liquid.

The electrical and thermal transport properties were measured over the temperature range from 300 to 600 K. The electrical conductivity was determined by four-probe AC technique. The Seebeck coefficient and thermal conductivity measurements were conducted in radiation-

shielded vacuum probe by forcing variable heat flux across the sample and measuring corresponding linear variations of temperature differences and thermoelectric voltage in steady-state conditions. Heat flux, passing by the cold side of the sample, was measured by previously calibrated heat-flux sensor. The results were used for precise calculations of increased heat losses due to very low thermal conductivity of measured samples. The Hall coefficient R_H was measured using low frequency (7 Hz) AC sample current of 50 to100 mA/mm^2 in a constant magnetic field of 0.705 T at the room temperature. Carrier concentrations were evaluated from the Hall coefficient R_H, assuming a Hall scattering factor A equal to 1.0.

Electronic structure computations have been performed using full potential Green function Korringa-Kohn-Rostoker method [15-17] in ordered approximants of AgSbX_2 (see, Sec. 3.1) as well as hypothetical AgX and SbX. To account for chemical disorder in NaCl-type $Ag_{1-x}Sb_xX$ alloys, the coherent potential approximation (CPA) has been incorporated. The crystal potential of *muffin-tin* form has been constructed within the LDA framework, using von Barth-Hedin parametrization for the exchange-correlation part. For well-converged charges and potentials, the total, site-decomposed and l-decomposed density of states (DOS) were computed applying k-space tetrahedron integration. The Fermi level was determined from the generalised Lloyd formula [18,19]. The electronic properties of fully disordered system within the NaCl-type structure, corresponding to the chemical formula $Ag_{0.5}Sb_{0.5}X$ (X= Se and Te), have been compared to those obtained in five ordered approximates, assuming different crystal structures, since all they resulted in very close X-ray diffraction patterns. Moreover, the origin of pseudo-gap properties of $AgSbSe_2$ and $AgSbTe_2$ systems has been better enlightened through electronic structure calculations of hypothetical end-point binary compounds AgX and SbX. In all calculations of selenides and tellurides, we employed the experimental values of lattice constants determined in $AgSbSe_2$ and $AgSbTe_2$, respectively.

3. Results and discussion

3.1. Structural analysis

Scanning electron microscopy (SEM) observations with simultaneous EPMA analysis of the samples revealed that the resulting materials had an uniform microstructure and chemical composition. The $AgSbTe_2$ samples contained well-formed grains with sizes ranging from 5 to 50 μm (Fig. 1a) . The $AgSbSe_2$ samples had a glass-like texture without visible grain borders (Fig. 1b). The measured densities were found to be 98% of the theoretical value. XRD analysis confirmed that obtained $AgSbSe_2$ samples were single–phased. In case of $AgSbTe_2$ only small amounts (appr. <3%) of secondary phase inclusions were observed.

The Rietveld method was used for refining of the structure parameters for the disordered NaCl structure model (*Fm3m*) as well as different models of ordered ABX_2 - type structures. There were considered the most common superstructures of NaCl: e.g. α̃-$NaFeO_2$ (*R-3m*), $LiTbS_2$ (*Fd-3m*) and γ̃-$LiFeO_2$ (*$I4_1$/amd*). The final results of refinement for the $AgSbSe_2$ material are presented in the Table 2.

Analysis of "goodness of fit" statistical parameters for the refinement results, such as: χ^2, R_{wp}, and Durbin-Watson statistics, show that all the models describe experimental data practically with the same precision and therefore they are indistinguishable by these criteria. Moreover, in all calculated, theoretical X-ray diffraction patterns, intensities of characteristic superstructure reflections are lower than the experimental background signal. These results are a consequence of very similar (different only of about 5%) *X*-ray scattering factors of Ag and Sb for CuK_α radiation. Therefore, it seems that the nature of ordering in the $AgSbSe_2$ and $AgSbTe_2$ structure can not be easily investigated by classical *X*-ray diffraction techniques. However, preliminary structural calculations show that such analysis would be possible by using neutron radiation method.

3.2. Transport properties

Studies of temperature dependences of electrical conductivity revealed that $AgSbSe_2$ and $AgSbTe_2$ exhibit semimetallic/semiconducting behavior. The activation energies E_a for both compounds, determined using an Arrhenius law, are about 0.03 eV and remain close to another result of 0.09 eV obtained from electrical investigations (Table 1). On the other hand, these data are much lower than values of direct band gap energy E_g^d (0.3 to 0.71 eV) measured by optical method for intrinsic absorption region. It may suggest that results of electrical investigations correspond rather to activation energy of extrinsic charge carriers, but another explanation of discrepancies may lay in significant differences in microstructure of samples (thin layer vs. bulk polycrystalline material).

The magnitude of the Seebeck coefficient of $AgSbTe_2$ at the room temperature is consistent with semimetallic behavior of this sample (68 μV K^{-1}). The Seebeck coefficient for $AgSbSe_2$ is much larger (320 μV K^{-1}) what can be an indication of more semiconducting-like character of this compound. Both materials exhibit *p*-type of conductivity and relatively large Hall concentration of carriers of $1 \cdot 10^{19}$ and $5 \cdot 10^{19}$ cm^{-3} for $AgSbSe_2$ and $AgSbTe_2$ respectively. The Seebeck coefficient and Hall carrier concentration data were used to estimation of effective mass of carriers m^*, assuming a single parabolic band model with acoustic phonon scattering as a predominant carrier scattering mechanism.

In this model, the Seebeck coefficient α can be expressed as follows:

$$\alpha = -\frac{k_B}{e}\left(\frac{2F_1(\eta)}{F_0(\eta)} - \eta\right) \tag{2}$$

The carrier concentration *n* can be expressed as follows:

$$n = 4\pi\left(\frac{2m^* k_B T}{h^2}\right)^{3/2} F_{1/2}(\eta) \tag{3}$$

where: k_B is the Boltzmann's constant, η - reduced Fermi energy, F_x - Fermi integral of order *x*, m^* - effective mass, T- absolute temperature.

At first, we calculated the reduced Fermi levels from the experimental Seebeck coefficient data using Eq. (2), then determined electron effective masses from Eq. (3) using the calculated reduced Fermi energies and the experimental Hall carrier concentration values.

The calculated effective masses of carriers are significantly different: 2.7 for $AgSbTe_2$ and 0.7 for $AgSbSe_2$, despite of comparable mobility (40-50 $cm^2s^{-1}V^{-1}$). Dissimilar effective masses m^* can indicate some differences in band structure of both compounds near the Fermi energy.

The samples of $AgSbSe_2$ and $AgSbTe_2$ exhibit very low thermal conductivity (see Table 3). The measured value for $AgSbSe_2$ at room temperature is with very good agreement with literature data (Table 1), whereas thermal conductivity of $AgSbTe_2$ is higher than earlier reported value (0.62 $W \cdot m^{-1}K^{-1}$). The discrepancy can be result of different amount of secondary phase inclusions and larger electrical conductivity.

Total thermal conductivity λ of solids is the sum of carrier $\lambda_{el.}$ and lattice λ_{latt} components:

$$\lambda = \lambda_{el} + \lambda_{latt} \qquad (7)$$

In order to explain impact of the electronic contribution on thermal conductivity, the Wiedemann-Franz-Lorenz law was applied and the values of thermal conductivity λ_{el} were estimated:

$$\lambda_{el} = LT\sigma \qquad (8)$$

where L is the Lorenz number which may vary from $1.485 \cdot 10^{-8}$ V^2K^{-2} for nondegenerated semiconductors to $2.443 \cdot 10^{-8}$ V^2K^{-2} for metals and for strongly degenerated semiconductors.

However, above Lorenz number are not applicable for partially degenerated semiconductors. Therefore, an attempt have been undertaken to determine the Lorenz number L and the electronic part of thermal conductivity with the use of Fermi-Dirac statistics as follows:

$$L = \frac{k_B}{e^2}^2 \left[\frac{r+3}{r+1} \cdot \frac{F_{r+2}(\eta)}{F_r(\eta)} - \left\{ \frac{r+2}{r+1} \cdot \frac{F_{r+1}(\eta)}{F_r(\eta)} \right\}^2 \right] \quad (9)$$

The Fermi level values, which were used in the above calculations, alike those of carrier effective masses, were estimated with the use of absolute Seebeck coefficient experimental data (Eq. 4.). The results of computations are presented in Table 3; they indicate that about 18% and 5% of the total thermal conductivity, for $AgSbTe_2$ and $AgSbSe_2$ respectively, can be contributed to its electronic part.

The thermoelectric figure of merit *ZT* which can be expressed as:

$$ZT = \frac{\alpha^2 \sigma}{\lambda_{el} + \lambda_l} T \quad (10)$$

is commonly used parameter for evaluation of thermoelectric materials.

Maximal values of *ZT* were measured at temperature of 525 K and are equal about 0.2 and 0.1 for $AgSbTe_2$ and $AgSbSe_2$ respectively. However, optimization of carrier concentration (e.g. by doping) should enhance properties of both materials.

3.3. Electronic structure

3.3.1 Binary compounds AgX and SbX

The investigations of electronic structure characteristics in hypothetical Ag*X* and Sb*X* allowed to get more insight into formation of semimetallic properties in $AgSbX_2$. From Fig. 4, presenting densities of states (DOS) in Ag*X* and Sb*X*, one learns that there is a deep valley (or a true energy gap) in the electronic spectra, above the 8th or 18th band in the case of Sb*X* and Ag*X*, respectively. Since the binary compounds possess the valence electron number (VEN) different from the aforementioned ones, i.e. VEN = 11 in Sb*X* and VEN = 17 in Ag*X*, they exhibit metallic ground state.

Electronic structure of Ag*X* consists of lower lying *s*-like states (containing 2 electrons), which comes essentially from *X* atom, and the block of presumably *d*-Ag and *p*-X states,

enabling to accommodate 16 electrons. The semiconducting or semimetallic properties would be expected if all these bands are completely filled (VEN = 18). Since Ag*X* possess 17 valence electrons (if accounting for *s*-*X* states), the Fermi level (E_F) is placed in upper region of the valence bands (VB). Consequently, Ag*X* (VEN=17) can be viewed as one-hole compounds, since one electron must be added to reach the true energy gap (or a deep DOS valley).

Electronic structure of Sb*X* consists of four successive blocks of bands. The lower lying two separate and narrow *s*-DOS peaks arrive from *X* (the lowest band) and Sb atoms. The higher lying two blocks of strongly hybridised *p*-states from *X* and Sb, are separated by a true gap or a deep DOS minimum seen in SbSe and SbTe, respectively. Hence, the semiconducting properties would be expected for VEN = 8 and then Sb*X* (VEN = 9) systems can be viewed as one-electron compounds due to the Fermi level falling at the bottom of the conduction band (CB). From the analysis of hypothetical binary parent compounds, we see that there is a slight difference between selenides and tellurides concerning electronic states near E_F, i.e. the presence of the energy gap separating VB and CB in AgSe and SbSe, whereas only a deep DOS minimum in AgTe and SbTe. This behaviour will have some consequences on differences in electronic structure of AgSbX_2.

3.3.2 Ternary ordered AgSbX_2

Our computations of different crystallographically ordered approximants of AgSbX_2 (resulting in the X-ray diffraction patterns similar to that received for disordered NaCl-type structure, see Table 4) show that their ground state electronic properties are really very close. In all considered cases, the Fermi level (E_F) was found either in the deep valley (semimetallic-like state) due to a small overlap of VB and CB, (Fig. 5) or it exhibits a pseudo-gap behaviour (VB and CB edges contact at E_F), depending on different atomic arrangements. Thus, the question whether AgSbX_2 may form superstructures different from NaCl-type alloy

should be addressed to the forthcoming neutron diffraction measurements as well as the accurate electronic structure computations including the analysis of the total energy. At the moment we focus more attention on electronic structure of the disordered model of AgSbX_2, which may serve as a reference case for further consideration of possible atomic superstructures. Noteworthy, the fully disordered model of AgSbX_2 is widely accepted in the literature.

3.3.3 Fully disordered $Ag_{0.5}Sb_{0.5}X$

The appearance of semimetallic properties in the NaCl-type disordered AgSbX_2 is not so straightforward from the aforementioned analysis (see, Sec. 3.3.1) of the binary parent compounds (and predictions of rigid band model). The Fermi level was supposed to fall into the gap at VEN = 8 or VEN = 18 (accounting for *d*-shell), which can be expected when adding/removing one or three electrons to/from AgX or SbX, respectively (antimony possesses four electrons more than silver). In $Ag_{1-x}Sb_xX$ alloy, Ag 4*d*-states are noticeably present in the valence band but they are almost completely filled, which can be detected from almost vanishing *d*-contribution to total DOS above E_F (Fig. 4). In Sb (Z = 51), due to more attractive crystal potential comparing to that of Ag (Z = 47), the 4*d*-states are practically expelled from the valence states (they form a semi-core levels) and only *sp*-states are present. Hence, the onset of pseudo-gap on DOS can not be expected neither at VEN = 8 nor at VEN = 18, due to specific hybridization of different type of orbitals (*d*-orbitals of Ag and *p*-orbitals of Sb) in alloyed system. Fig. 5 illustrates the DOS evolution in $Ag_{1-x}Sb_xX$, which can not be interpreted in terms of rigid band behaviour and a simple shift of E_F with the variation of the number of valence electrons. Since the change in the relative Ag/Sb content strongly modifies the population of *d*-type Ag and *sp*-type Sb orbitals (and also their hybridization), one can establish the simple rule for appearance of the pseudo-gap at the Fermi level in $Ag_{0.5}Sb_{0.5}X$ from the following relation : VEN = 0.5 x 11 [*sd*-Ag] + 0.5 x 5 [*sp*-Sb] + 6 [*sp*-Se], yielding

VEN=14. The above-mentioned VEN rule is in line with the simple ionic condition leading to a saturation of chemical bonds and then an onset of the semiconducting state in $AgSbX_2$ system, if accounting for the expected valence states of the constituent atoms, i.e. Ag^{+}, Sb^{+3} and X^{-2}. The energy gap above the 7th band in $Ag_{0.5}Sb_{0.5}X$ was partly confirmed in view of accurate KKR-CPA computations (Fig. 6). However, our results rather indicate a pseudo-gap behaviour than the appearance of the band gap at E_F in both compounds. Furthermore, the evolution of DOS in both series of compounds shows subtle differences, since $Ag_{0.5}Sb_{0.5}Te$ exhibits slightly higher DOS value at E_F than $Ag_{0.5}Sb_{0.5}Se$. This feature well corroborates with electronic properties detected in binary (true energy gap in selenides against a deep valley in tellurides). Interestingly, more 'metallic-like' character of $Ag_{0.5}Sb_{0.5}Te$ (lower thermopower and electrical resistivity) with respect to $Ag_{0.5}Sb_{0.5}Se$ was observed from our electron transport properties measurements.

However, accurate investigations of the Fermi surface properties (including computations of k-dependent electron group velocities and life-times [20]) are necessary to obtain more quantitative insight into the thermopower behaviour of these compounds.

4. Conclusions

We have studied the crystallographic and physical properties of $AgSbSe_2$ and $AgSbTe_2$ polycrystalline samples. Structural analysis using Rietveld refinement method shows that the nature of the disorder can not be handling by X-ray powder diffraction method due to similar scattering factors for Ag and Sb atoms. However, preliminary calculations show that such analysis would be possible by using neutron radiation method, what will be undertaken in further investigations.

Both compounds exhibit promising thermoelectric properties, in particular very low thermal conductivity and quite large, positive Seebeck coefficient. Temperature dependence

of electrical conductivity points out semiconducting with a very narrow band (E_g ~ 30 meV) or semimetallic properties of these materials. The $AgSbSe_2$ and $AgSbTe_2$ compounds exhibit *p*-type conductivity, what suggests that Fermi level is shifted on the valence bands edge.

The electronic structure calculations in fully disordered as well as in different ordered models of $AgSbX_2$ confirm practically in all cases that their ground state properties are semimetallic due to a slight overlapping of conduction and valence bands near the Fermi energy. Interestingly, in $AgSbSe_2$ the calculated DOS value is about twice smaller than the corresponding value in $AgSbTe_2$. All the DOS features well support electrical resistivity measurements exhibiting ρ weakly dependent with T (resulting in the activation energy gap close to zero in both systems) as well as the ρ values larger for $AgSbSe_2$. Moreover, the measured RT thermopower, which is much larger in $AgSbSe_2$ (α = 320 μV K^{-1}) than in $AgSbTe_2$ (α = 68 μV K^{-1}), can be related to relatively stronger variation of valence-like DOS as well as lower $N(E_F)$ in the former.

Besides, we suggest that the presence of low DOS near E_F in $AgSbX_2$ allows easily tuning the Seebeck coefficient sign upon suitable doping/substitution. However, *n*-type $AgSbX_2$ compounds are expected to have smaller thermopower than the presented here *p*-type materials, as can be roughly detected on the KKR-CPA DOS.

Acknowledgments

The work was supported by The EEA Financial Mechanism & The Norwegian Financial Mechanism, (grant No PL0089-SGE-00104-E-V2-EEA, 2007-2010).

References

[1]. S. Geller, J. H. Wernick, „Ternary Semiconducting Compounds witch Sodium Chloride-Like Structure: $AgSbSe_2$, $AgSbTe_2$, $AgBiS_2$, $AgBiSe_2$". Acta Cryst. 12 (1959) 46.

[2]. J.H. Wernick, New semiconducting ternary compounds", Phys. Soc. 21, 1957

[3]. R. Wolfe, J.H. Wernick, E. Haszko, Anomalous Hall Effect in $AgSbTe_2$, J. Appl. Phys., 31, 1960, 1959-1964

[4]. K. Wang, C. Steimer, R. Detemple, D. Wamwangi, M. Wutting, "Assessment of Se-based phase change alloy as a candidate for non-volatile electronic memory applications" Appl. Phys. A81, (2005) 1601-1605.

[5]. J. Xu, B. Liu, Z. Song, S. Feng, B. Chen, "Crystallization and C-RAM application of Ag-doped Sb_2Te_3 material" Materials Science and Engineering B 127 (2006) 228-232

[6]. H.A. Zayed, A.M Ibrahim, L.I Soliman, "Optical absorption behavior of $AgSbTe_2$ thin films" Vacuum. Vol. 47, No. 1, (1996) 49-51

[7]. H. S. Soliman, D. Abdel-Hady, E. Ibrahim, "Optical properties of thermally vacuum evaporated $AgSbSe_2$ thin films" J. Phys.: Condens. Matter 10 (1998) 847-856 (UK).

[8]. K. Wand, C. Steimer, M. Wutting, "Phase change properties of ternary $AgSbSe_2$ chalcogenide films" Journal of Ovonic Research 2, (4) (2006) 61-65.

[9]. A.R. Patel and D.Lakshminarayana, "Effect of Substrate Temperature On the Crystalline of $AgSbSe_2$ Films", Thin Solids Films, 98 (1982) pp 59-63

[10]. A. Abdelghany, S.N. Elsayed, D.M. Abdelwahab, A.H. Abou El Ela, N.H Mousa: Electrical conductivity and thermoelectric power of $AgSbSe_2$ " Mat. Chem. and Phys. 44 (1996) 277-280

[11]. A. R. Patel D. Lakshminarayana and K. V. Rao, "Growth and Crystallization of $AgSbSe_2$ Films". Thin Solids Films, 98 (1982) 51-57.

[12]. D. M. Rowe, ed., Handbook of Thermoelectrics, CRC Press, Boca Raton, FL, 1994

[13]. N. Chen, F. Gascoin, G. J. Snyder, E. Müller, G. Karpinski, C. Stiewe, "Macroscopic thermoelectric inhomogeneities in $(AgSbTe_2)_x(PbTe)_{1-x}$" Appl. Phys. Lett. 87, 171903 (2005)

[14]. Ravhi S. Kumar, A. Sekar, N. Victor Jaya, S. Natarajan "Synthesis and high pressure studies of the semiconductor $AgSbSe_2$" J. of Alloys and Compd. 285 (1999) 48-50.

[15]. S. Yoneda, Y. Ohno, E. Ohta, N. Yuhashi, I. Siota, Y. Shinohara, H.T Kaibe, I.A Nishida. "Temperature dependence of the figure-of-merit of "$Ag_{0,208}Sb_{0,275}Se_{0,517}$" 21st International Conference on Thermoelectrics (2002).

[16]. A. Bansil, S. Kaprzyk, P.E. Mijnarends, J. Tobola, "Electronic structure and magnetism of $Fe_{3-x}V_xX$ (X=Si, Ga, and Al) alloys by the KKR-CPA method", Phys. Rev. B **60** (1999) 13396.

[17]. K. T. Wojciechowski, J. Tobola, J. Leszczynski, "Thermoelectric properties and electronic structure of $CoSb_3$ doped with Se and Te", J. Alloys Compd. 361 (2003) 19.

[18]. T Stopa , S Kaprzyk , J Toboła , "Linear aspects of the Korringa–Kohn–Rostoker formalism", J. Phys.: Condens. Matter **16** (2004) 4921.

[19]. S. Kaprzyk and A. Bansil, "Green's function and a generalized Lloyd formula for the density of states in disordered muffin-tin alloys", Phys. Rev. B **42**, (1990) 7358.

Table 1 Selected physical properties of $AgSbSe_2$ and $AgSbTe_2$.

Parameter	$AgSbTe_2$	$AgSbSe_2$
Space group	Fm3m	Fm3m
Cell size [Å]	6.078 [1]	5.786 [1]
Density [$g \cdot cm^{-3}$]	7.12 [1]	6.60 [1]
Band gap [eV]	0.71** [6] 1.65*** [6]	0.091* [11] 0.34* [10] 1.03*** [7]
Thermal conductivity [$W \cdot m^{-1} \cdot K^{-1}$]	0.64 [3]	0.82 [9]
Electrical conductivity [$S \cdot cm^{-1}$]	130-150 [3]	154 [14]
Seebeck coeff. [$\mu V \cdot K^{-1}$]	165-240 [3]	
Melting point [°C]	555 [2]	610 [2]

* electrical measurements; ** direct gap - optical measurements;
*** indirect gap - optical measurements

Table 2. Results of Rietveld refinement for the disordered structure (Fm3m) and selected possible ordered systems of $AgSbSe_2$.

Short-range order	s.g.	a [Å]	b [Å]	c [Å]	χ^2	R_{wp}	DW-stat.
disordered	Fm3m	5.7883	-	-	2.15	27.3	0.51
Superstructures (short-range ordered structures)							
A1	R-3m	4.0933	4.0933	20.0475	2.25	28	0.48
B1	Fd-3m	11.5766	-	-	2.15	27.3	0.51
F1	$I4_1/amd$	5.7883	5.7883	11.5766	2.25	28	0.48
E1	Pmmn	5.7883	-	-	2.15	27.3	0.50

Table 3. Thermoelectric properties of undoped $AgSbTe_2$ and $AgSbSe_2$ samples at room temperature.

Parameter	**$AgSbTe_2$**	**$AgSbSe_2$**
Cell size a [Å]	6.0816	5.7883
Density ρ [g·cm^{-3}]	7.15	6.60
Band gap E_g [meV]	26	30
Electrical conductivity σ [S·cm^{-1}]	332	79
Seebeck coeff. [μV·K^{-1}] (at 320 K)	68	320
Thermal conductivity λ [W·m^{-1}·K^{-1}]	1.15	0.81
Elec. contr. of therm. conduct. λ_{el} [W·m^{-1}K^{-1}]	0.2	0.04
Type of majority carriers	*p*	*p*
Hall carrier concentration n [cm^{-3}]	$5.0 \cdot 10^{19}$	$1.0 \cdot 10^{19}$
Hall mobility μ [cm^{2}s^{-1}V^{-1}]	41	49.2
Carrier effective mass m*/m$_0$	2.7	0.7
ZT parameter (at 525 K)	0.2	0.1

Table 4 Results of computations for the disordered structure (Fm3m) and selected possible ordered systems of $AgSbSe_2$.

Short-range order	**s.g.**	**Band gap E_g**	**Position of the Fermi level E_f**
disordered	Fm3m	semimetal	minimum of DOS
A1 B1	R-3m Fd-3m	semimetal ~0.1 eV	valence bands minimum of DOS
F1	$I4_1/amd$	semimetal	conduction bands
E1	Pmmn	semimetal	valence bands

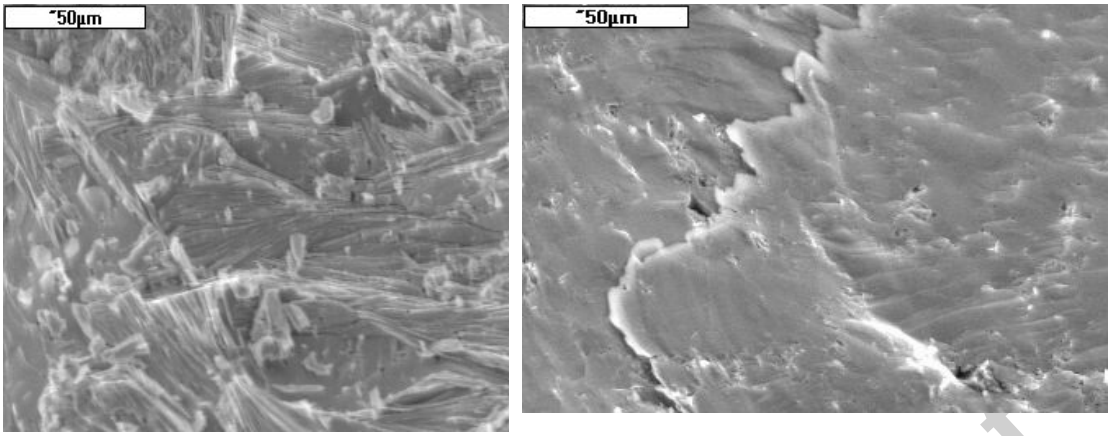

a) b)

Fig. 1 SEM picture of the fracture of a) $AgSbTe_2$ and b) $AgSbSe_2$ sample.

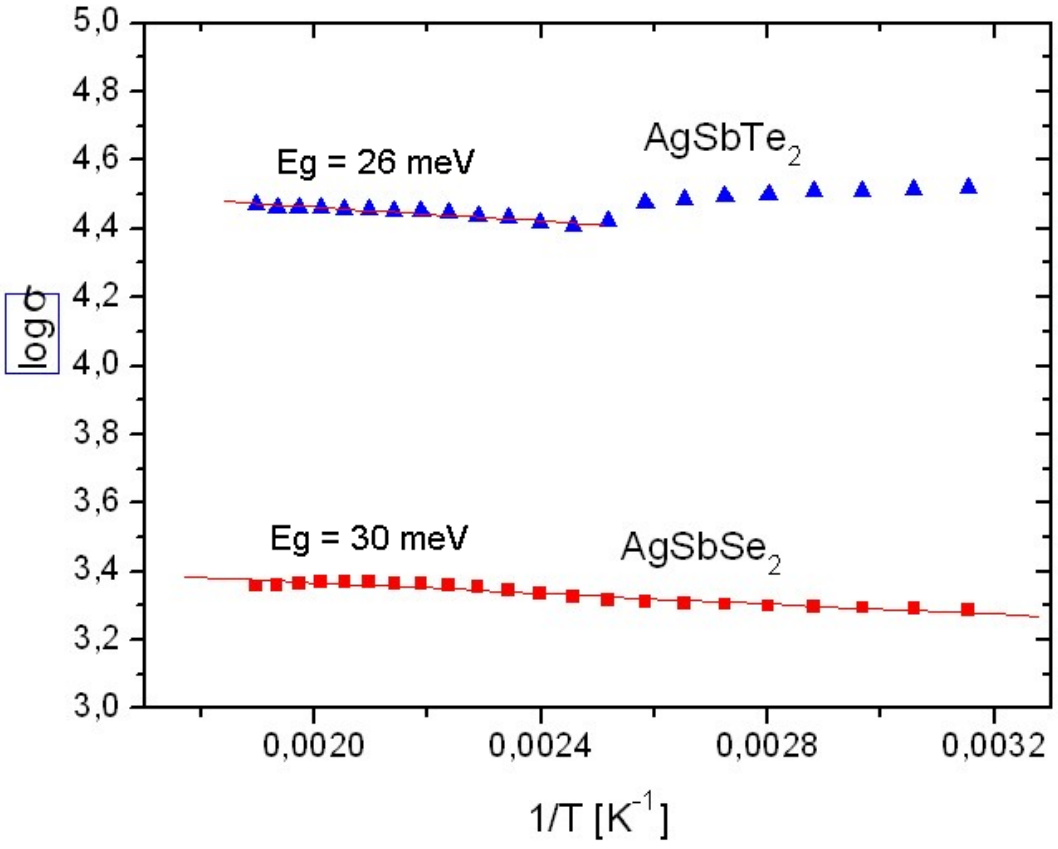

Fig. 2 Temperature dependence of electrical conductivity of $AgSbSe_2$ and $AgSbTe_2$.

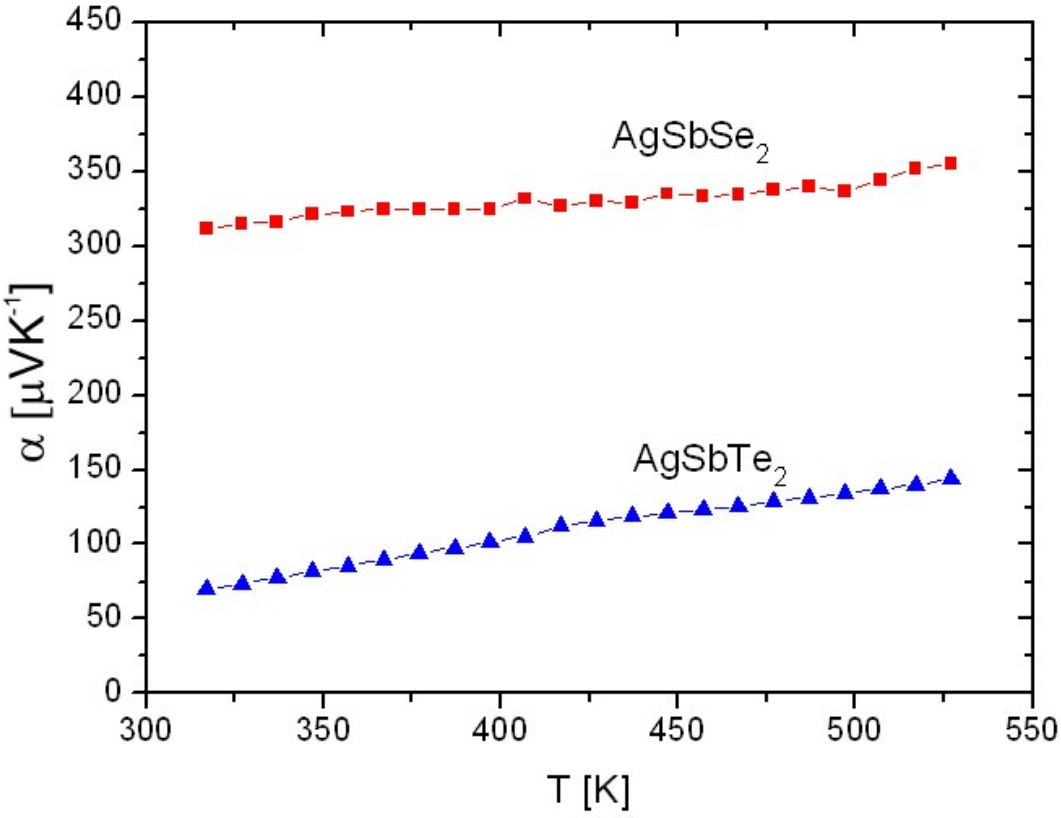

Fig. 3 Temperature dependence of the Seebeck coefficient values of $AgSbSe_2$ and $AgSbTe_2$.

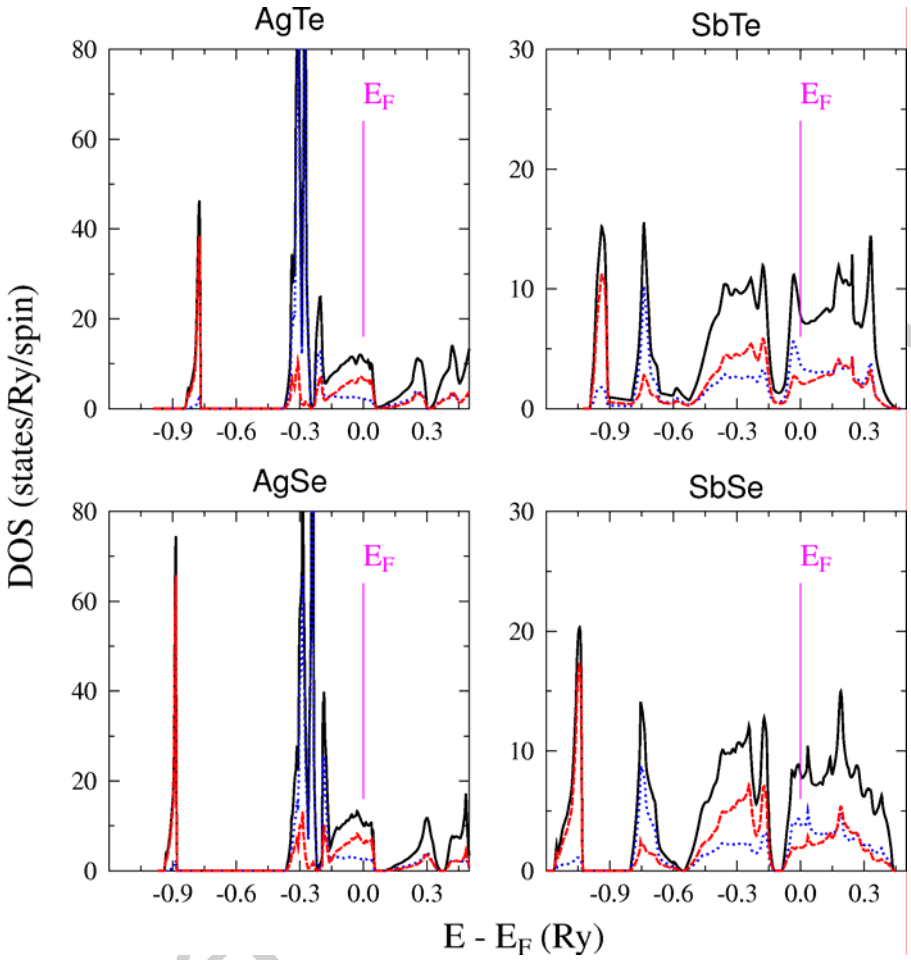

Fig. 4 DOS of hypothetical NaCl-type parent compounds AgSe, AgTe, SbSe and SbTe. Black (solid), blue (dot) and red (dash) lines represent total, 'left' (Ag, Sb) and 'right' (Se, Te) DOS, respectively.

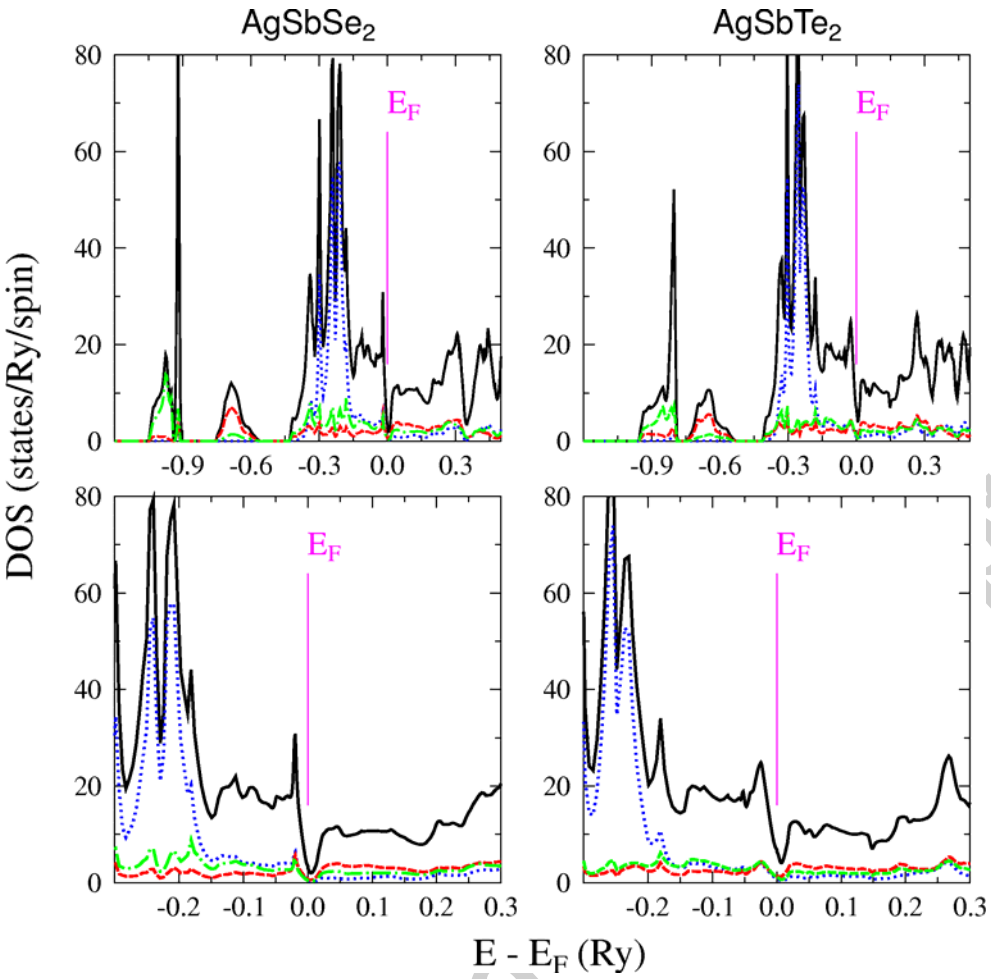

Fig. 5 DOS of the illustrative ordered approximate (E1, s.g. *Pmmn*) of $AgSbSe_2$ (left panel) and $AgSbSe_2$ (right panels). Black (solid), blue (dot), red (dash) and green (dot-dash) lines represent total, Ag, Sb and *X* DOS contributions, respectively. In lower panels only electronic E_f are enlarged.

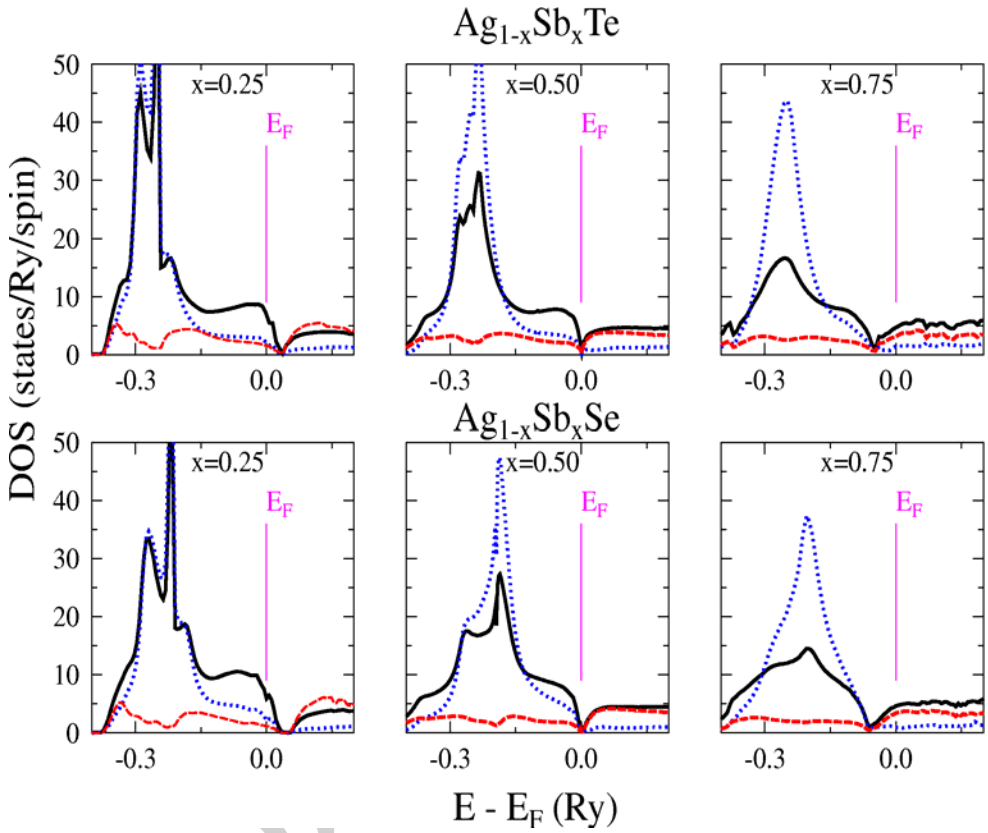

Fig. 6 Evolution of KKR-CPA DOS near the Fermi level in the disordered (NaCl-type) $Ag_{1-x}Sb_xSe$ (a) and $Ag_{1-x}Sb_xTe$ (b). Total, Ag, Sb and Se DOS contributions are plotted by a black (solid), blue (dot), red (dash) and green (dot-dash) lines, respectively.